CANCER BIOLOGY & THERAPY
2019, VOL. 20, NO. 6, 897–911
https://doi.org/10.1080/15384047.2019.1579960

Taylor & Francis
Taylor & Francis Group

RESEARCH PAPER

MicroRNA-23a depletion promotes apoptosis of ovarian cancer stem cell and inhibits cell migration by targeting DLG2

Ru-Jin Zhuang, Xiao-Xu Bai, and Wei Liu

Department of Obstetrics and Gynecology, The Second Affiliated Hospital of Harbin Medical University, Harbin, P.R. China

ABSTRACT

Ovarian cancer (OC) is xenogeneic that is influenced by many generated factors related to epigenetic factors to accelerate tumor metastasis. This study was conducted with the objective of investigating the effect of microRNA-23a-3p (miR-23a) on the biological characteristics of OC stem cells by targeting discs large homolog 2 (DLG2). OC-related differentially expressed genes were screened by microarray-based gene expression analysis, after which a list of miRNAs that regulate the genes was predicted. In total, 50 patients diagnosed with OC were enrolled in this study. DLG2 positive protein expression was measured in OC tissues. The interaction between DLG2 and miR-23a was predicted and analyzed through luciferase activity measurement. With the intervention of miR-23a and/or DLG2 expression in OC stem cells, the expression of miR-23a, DLG2, Bax, Bcl-2, Oct-4, and Nanog was determined. Afterward, different cell experiments were conducted to examine the regulation effect of miR-23a in OC stem cells. Tumor formation *in vivo* was also evaluated in nude mice. DLG2 had low expression in OC. The results showed that there was a decrease in the expression of Bcl-2, Oct-4, and Nanog, while DLG2 and Bax were increased as a result of miR-23a depletion. In addition, when miR-23a was suppressed, cell viability, migration, invasion, cloning, and renewal abilities of OC stem cells were decreased, while apoptosis ability was enhanced. As a target gene of miR-23a, DLG2 downregulation reversed the suppressive function of miR-23a in the inhibition of OC development. Finally, *in vivo* experiment verified that miR-23a downregulation restrained the tumor growth in OC stem cells. In conclusion, our findings suggested that the inhibition of miR-23a results in the suppression of OC progression by releasing DLG2, which provides new understanding on the potential therapeutic effect of miR-23a inhibition in OC patients.

ARTICLE HISTORY
Received 13 September 2018
Revised 19 November 2018
Accepted 3 February 2019

KEYWORDS
MicroRNA-23a-3p; discs large homolog 2; ovarian cancer; apoptosis; tumor stem cells

Introduction

Ovarian cancer (OC) is the seventh most frequently occurring cancer in women and characterized by a high mortality rate of up to 40–50%, due to the fact that most OC cases are diagnosed in the late stage.[1,2] OC is xenogeneic and influenced by generated factors related to epigenetic factors, as well as several chemokines and cytokines interacting with each other to accelerate the metastasis of OC cells.[3] Most malignant ovarian tumors may originate from the surface epithelium and/or fallopian tube of the ovary, out of which more than 90% are carcinomas, with a poor prognosis and a low overall 5-year survival rate.[4] The low long-term survival rate of this disease is due to the asymptomatic onset of the disease in early stages, the lack of minimally invasive methods for early examination, and the development of chemo-resistance therapies.[5] Therefore, there is an urgent need in finding more effective therapeutic options for OC patients. A number of molecular studies have supported a conception that different histological types of OC are likely to exhibit distinct histopathological, genetical, and biological characterization.[6]

MicroRNAs (miRNAs) play a significant role in the regulation of different kinds of biological processes such as cell development, differentiation, proliferation, and apoptosis.[7] Lately, miRNA dysregulation has been reported to be linked to an increase in oncogenicity and poor prognosis in some types of cancer, such as osteosarcoma.[8] miR-23a, a miRNA highly conserved across species, plays a major role in the pathophysiology of various kinds of diseases.[9] A study has reported that miR-23a could be a contributor to cancer cell and stem cell migration and invasion in colorectal cancer.[10] Upregulated miR-23a enhances tumorigenic activity by promoting the development of cell cycle and suppressing cell apoptosis in OC cells.[11] Based on the findings from miRNA target prediction, discs large homolog 2 (DLG2) was found to be a target gene of miR-23a. DLG2 is a membrane-related protein that is a member of the MAGUK family.[12,13] DLGs are known to have various protein–protein interaction domains, which can form different protein complexes and therefore, have a wide range of cellular functions.[14] A previous study by Wu *et al.* demonstrated that *DLG2* gene variant was associated with the risk of Parkinson's disease.[12] The aforementioned findings led to the hypothesis that miR-23a and DLG2 may be involved in OC progression and therefore, we conducted the following study to determine the biological functions of miR-23a in OC stem cells with a regulation effect on DLG2.

CONTACT Wei Liu liuwei19780716@126.com Department of Obstetrics and Gynecology, The Second Affiliated Hospital of Harbin Medical University, No. 246, Xuefu Road, Nangang District, Harbin, Heilongjiang Province 150086, P.R. China

Results

DLG2 is a potential target of miR-23a in OC cells

The differentially expressed genes (DEGs) were screened from the OC gene chips GSE14407 and GSE38666 with *adj.P.Val* < 0.05 and |LogFoldChange| > 2 regarded as the screening criteria. The screening generated 176 and 158 DEGs from GSE14407 and GSE38666, respectively, and the top 20 DEGs from both chip datasets were compared using a Venn diagram (Figure 1(a)). In total, 14 intersection genes were found, including *NELL2, ARHGAP18, REEP1, TXNIP, AQP9, PDGFD, ITLN1, RERG, MMP28, DLG2, ZWINT, EFEMP1, AOX1*, and *ABCA8*. Meanwhile, the DigSee engine was searched for OC-related genes, and the top 15 genes were selected as potential OC-related disease genes, which consisted of *BRCA1, TP53, PLOD1, MUC16, BRCA2, VEGFA, ERBB2, FSHR, AKT1, SHBG, ESR1, EGFR, MAPK1, Bcl-2*, and *IGF1*. Based on the list of OC DEGs and OC-related disease genes found in the protein-protein information from the String database, a network of OC DEGs and disease genes was constructed (Figure 1(b)). In this network, we found that *TXNIP* and *PDGFD* were closely associated with OC disease genes and *DLG2* was linked to both OC disease genes and other DEGs. In addition, we performed the KEGG enrichment analysis on the DEGs and disease genes and the results (Figure 1(c)) showed that there were multiple cancer-related pathways, in which *PDGFD* was also enriched in the pathways related to prostate cancer and melanoma. Furthermore, *TXNIP* has been proposed to be a tumor suppressor gene.[15] Although differentially expressed *DLG2* was found in renal oncocytoma,[16] the significance and molecular mechanism of *DLG2* in OC were still unclear. As depicted in the heatmaps of the top 20 DEGs of GSE14407 and GSE38666 chips (Figure 1(d–e)), we found that the expression of *DLG2* was lower in OC tissues than in healthy tissues. To further investigate the molecular mechanism of *DLG2* in OC cells, miRDB, DIANA, miRWalk, mirDIP, TargetScan, and microRNA databases were used to predict miRNA candidates that regulate *DLG2*. As a results, 117 miRNAs were obtained from MiRDB database with Target Score ≥75, 54 miRNAs with miTG score ≥0.95 from DIANA database, 1750 miRNAs with energy <-20 from miRWalk database, 89 miRNAs with integrated Score ≥0.5 from mirDIP database, 56 miRNAs with conserved *DLG2* binding sites from TargetScan, and 55 miRNAs from microRNA database. The top 100 miRNAs from miRWalk were compared with other predictions using Venn diagram, which found one intersection between miRNA and hsa-miR-23a-3p (miR-23a for short) suggesting that miR-23a was very likely to interact with DLG2 (Figure 1(f)).

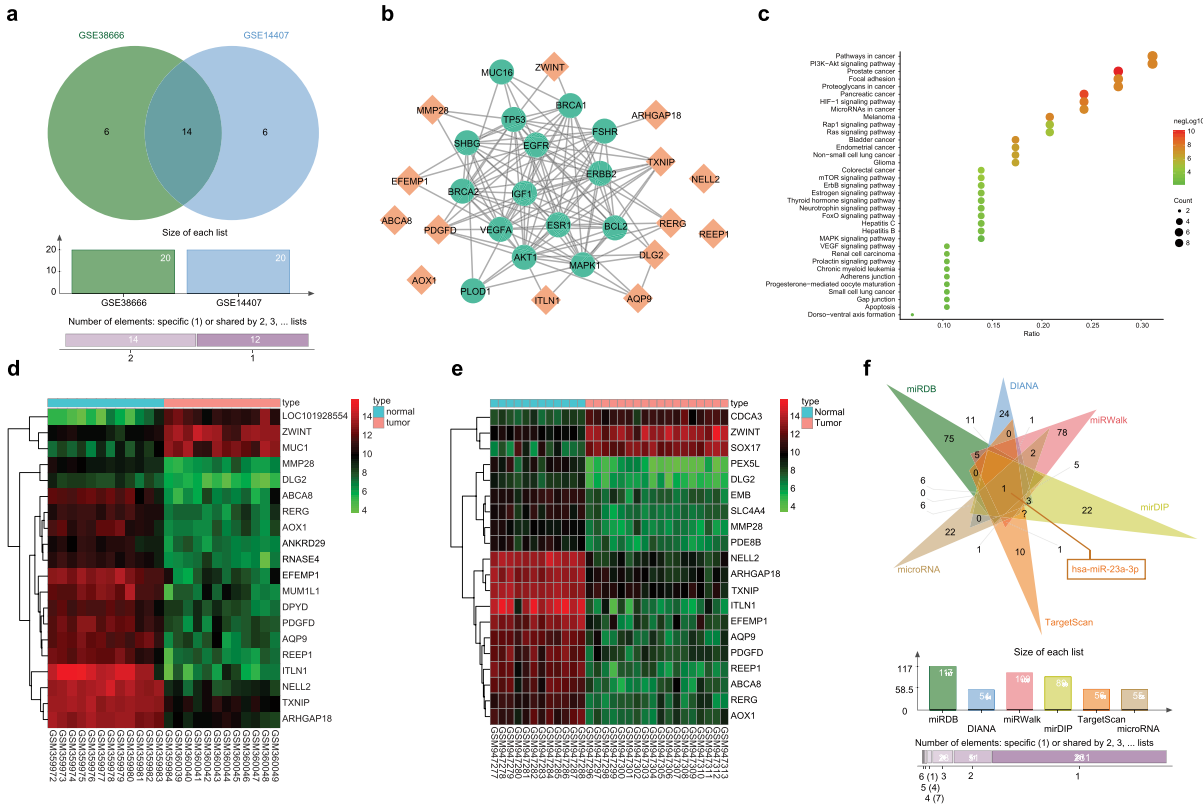

Figure 1. DLG2 is a potential regulation target of miR-23a. (a) 14 DEGs were found in the intersection between the top 20 DEGs from the OC chips GSE14407 and the top 20 DEGs from GSE38666; (b) the interaction network between DEGs and disease genes in OC, orange represents DEGs, and green represents disease genes; (c) KEGG enrichment results of OC DEGs and disease genes; (d) the heatmap of the top 20 DEGs of the OC chip GSE14407; the heatmap of the top 20 DEGs of the OC chip GSE38666. The abscissa indicates the sample number, the ordinate indicates DEGs, and the upper right histogram indicates the color gradation. Each rectangle corresponds to a sample expression value; (f) miRDB, DIANA, miRWalk, mirDIP, TargetScan, and microRNA were used to predict miRNAs that may regulate DLG2. miR-23a-3p, microRNA-23a-3p; DEG, differentially expressed gene; DLG2, discs large homolog 2; OC, ovarian cancer.

DLG2 has low positive protein expression in OC tissues

Immunohistochemistry was used to detect the positive expression of DLG2, which displayed cytoplasmic brownish or strongly brownish yellow (Figure 2(a)). The positive rate of DLG2 protein expression in the adjacent normal tissue was 77.23%, which was significantly higher than that in the OC tissue (23.06%) ($p < 0.05$, Figure 2(b)). In addition, the results of reverse transcription quantitative polymerase chain reaction (RT-qPCR) showed that compared with the adjacent normal tissue, the OC tissue showed a higher miR-23a expression ($p < 0.05$; Figure 2(c)).

The expression of miR-23a was significantly increased in OC stem cells

Flow cytometry was employed to conduct cell sorting. Before sorting, the proportion of $CD133^+$ cells was 4.12% and the expression rate of CD133 in the positive cell population by magnetic bead sorting was 82.52%, suggesting that the cells obtained by the magnetic cell sorting had a relatively high purity (Figure 3(a)). The result of immunofluorescence showed that the cell spheres, which consisted of $CD133^+$ cells, were mainly distributed on the cell membrane and expressed in the cytoplasm in a small amount (Figure 3(b)). The cells were observed under an inverted microscope, and the findings showed that cells were grown to a spherical cell body floating in a six-well plate (Figure 3(c)). The expression of miR-23a in $CD133^+$ and $CD133^-$ cells after sorting was quantified by RT-qPCR, and the results showed that the expression of miR-23a was significantly higher in the sorted $CD133^+$ cells than in the $CD133^-$ cells ($p < 0.05$) (Figure 3(d)).

DLG2 is a target gene of miR-23a

The online analysis platform (http://www.microrna.org) predicted that there was a specific binding region in the sequence of *DLG2* gene and miR-23a, indicating that *DLG2* was a target gene of miR-23a (Figure 4(a)). The results of dual-luciferase reporter gene assay (Figure 4(b)) confirmed this hypothesis, which showed that compared with the NC + DLG2-WT group, the luciferase activity was decreased in the miR-23a mimic + DLG2-WT group ($p < 0.05$); whereas, there was no significant difference in the luciferase activity of the mutant 3′UTR in the miR-23a mimic + DLG2-MUT ($p > 0.05$), indicating that miR-23a could specifically bind to *DLG2* gene and inhibit its expression.

Bcl-2, Oct-4, and Nanog were downregulated while DLG2 and Bax were upregulated by miR-23a inhibition

miR-23a mimic, miR-23a inhibitor, and siRNA-DLG2 were introduced into OC stem cells in order to explore the roles of

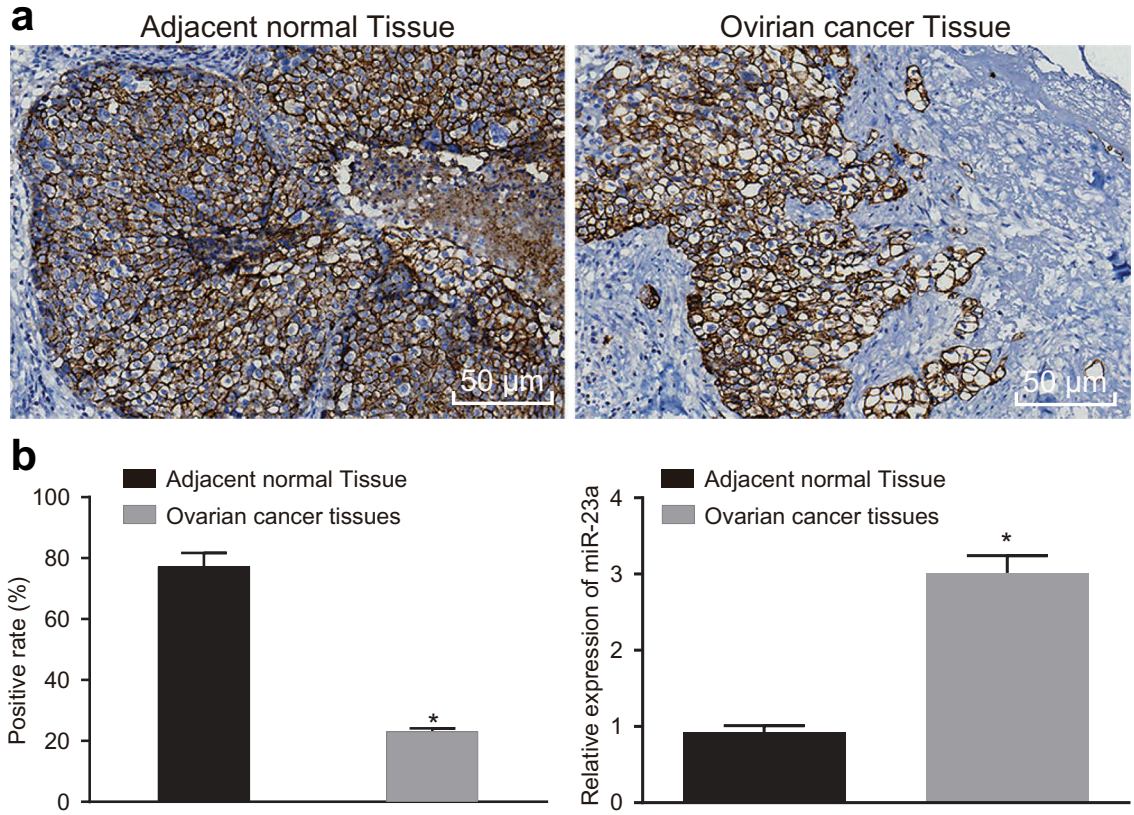

Figure 2. Positive rate of DLG2 protein expression in OC tissues is lower than in the adjacent normal tissues. (a) the images of DLG2 positive protein expression shown by immunohistochemical staining (× 200); (b) the positive rate of DLG2 protein expression in adjacent normal and OC tissues; (c) the miR-23a expression of the OC and adjacent normal tissues detected by RT-qPCR; *, $p< 0.05$, compared with the adjacent normal tissue. Data were analyzed by unpaired t-test, the experiment was repeated three times. DLG2, discs large homolog 2; OC, ovarian cancer; miR-23a, microRNA-23a; RT-qPCR, reverse transcription quantitative polymerase chain reaction.

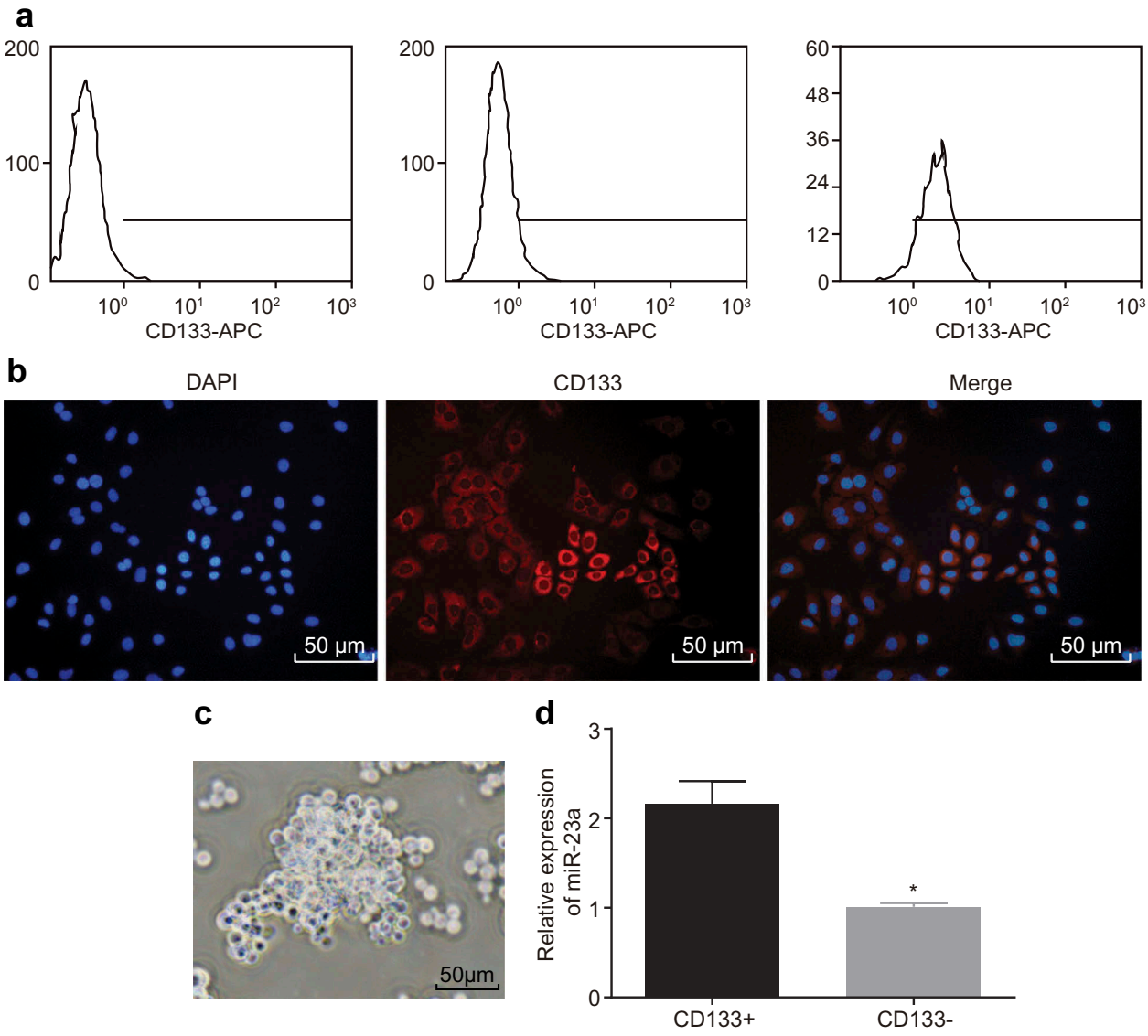

Figure 3. The expression of miR-23a was significantly increased in OC stem cells in comparison to that of the normal cells. (a) flow cytometry was used to verify the sorting efficiency of $CD133^+$ (a: isotype control, b: pre-sorting, c: post-sorting); (b) positive expression of CD133 protein (repeated three times); (c) $CD133^+$ cells growing in spherical shape in serum-free medium under an inverted microscope (×200); (d) the expression of miR-23a in $CD133^+$ and $CD133^-$ cells, as detected by RT-qPCR. The data were expressed as mean ± standard deviation and compared using *t*-test. The test was repeated three times. RT-qPCR, reverse transcription quantitative real-time polymerase chain reaction; miR-23a, microRNA-23a-3p; DAPI, 4′,6-diamidino-2-phenylindole; OC, ovarian cancer.

miR-23a and *DLG2* in OC. RT-qPCR and western blot analysis were employed to detect the expression of miR-23a, DLG2, and OC-related genes following several kinds of treatments on OC stem cells. The results (Figure 5(a–b)) showed that the miR-23a inhibitor + siRNA-DLG2 group had lower miR-23a expression than the blank and negative control (NC) groups ($p < 0.05$), while there was no significant difference observed in the mRNA and protein expression of DLG2, Bax, Bcl-2, Oct-4, and Nanog (all $p > 0.05$). In contrast to the blank group and the NC group, the expression of miR-23a in the miR-23a mimic group was increased significantly, the mRNA and protein expression of Bcl-2, Oct-4, and Nanog was enhanced, but the mRNA and protein expression of DLG2 and Bax was decreased (all $p < 0.05$). In comparison to the blank group and the NC group, there was a significant reduction in the expression of miR-23a in the miR-23a inhibitor group, a decrease in Bcl-2, Oct-4, Nanog mRNA and protein expression and an increase in DLG2 and Bax mRNA and protein expression (all $p < 0.05$). There was no significant difference regarding the expression of miR-23a in the siRNA-DLG2 group ($p > 0.05$) in comparison with the blank and NC group, but the mRNA and protein expression of Bcl-2, Oct-4, and Nanog was raised while those of DLG2 and Bax were declined (all $p < 0.05$).

OC stem cell proliferation, migration, and invasion were suppressed by miR-23a inhibition

In order to further analyze the effect of miR-23a in OC, OC cells were intervened with upregulation and downregulation of miR-23a or silencing of DLG2, and the cell viability was assessed with the use of the CKK-8 assay. The results (Figure 6(a)) showed that the miR-23a inhibitor + si-DLG2 group had no significant difference in cell viability at any time point compared with the

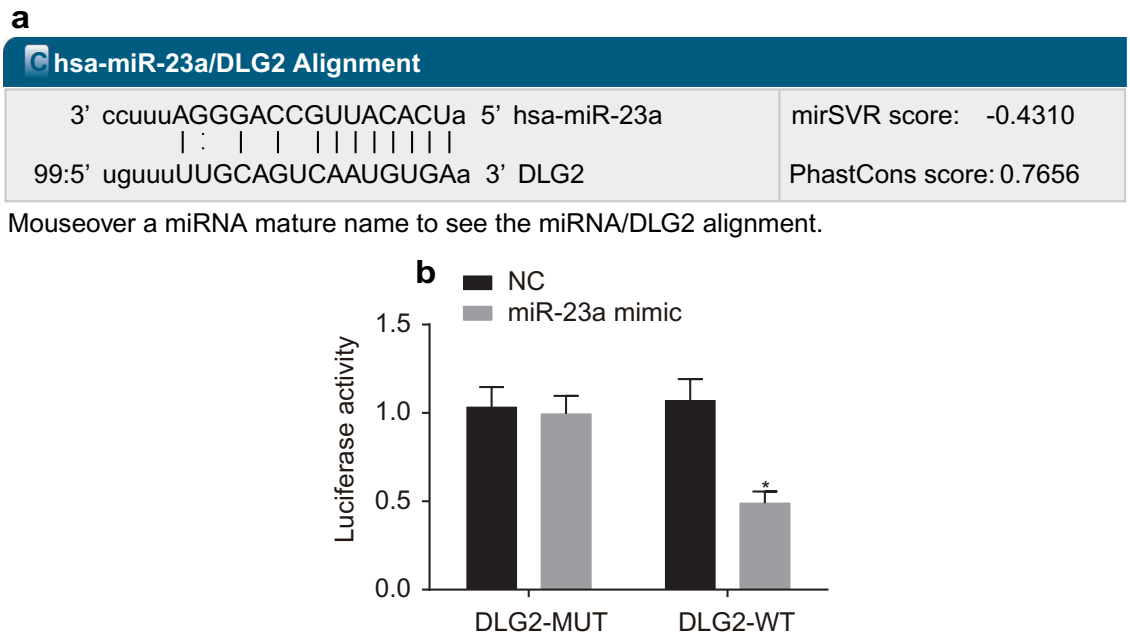

Figure 4. miR-23a negatively regulated the expression of DLG2. (a) the predicted binding site of miR-23a in DLG2-3′UTR; (b) the luciferase activity with miR-23a mimic + DLG2-WT co-transfection, determined by dual-luciferase reporter gene assay; *, $p< 0.05$, compared with the NC group (p value was obtained by t-test, and experiment was repeated three times). miR-23a, microRNA-23a-3p; DLG2, discs large homolog 2; NC, negative control.

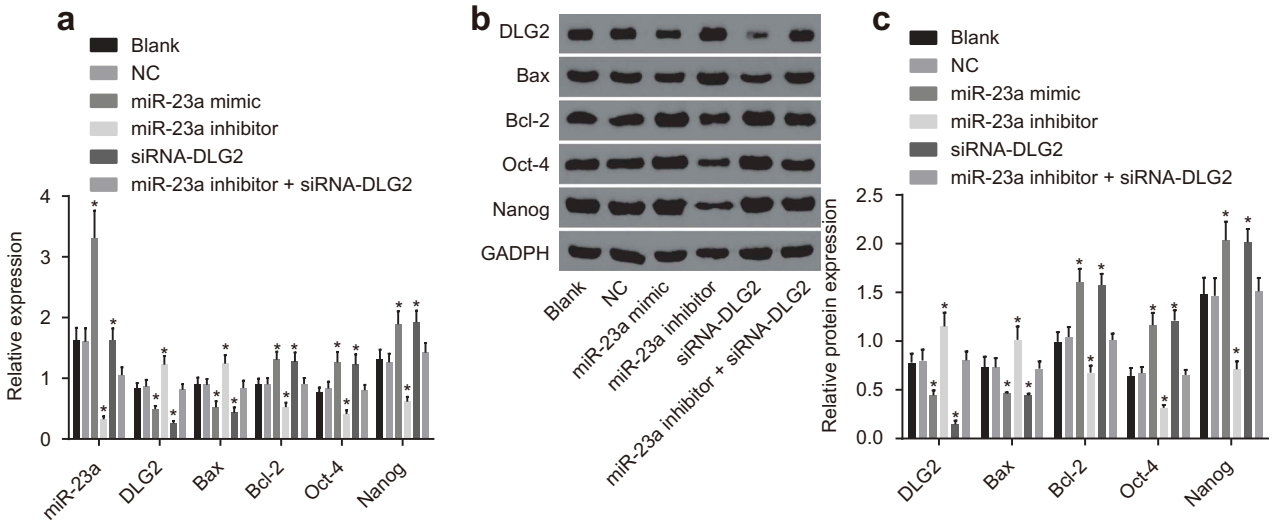

Figure 5. The mRNA and protein expression of Bcl-2, Oct-4 and Nanog was reduced but that of DLG2 and Bax was increased by downregulation of miR-23a. (a) The miR-23a expression, and mRNA expression of Bcl-2, Oct-4, Nanog, DLG2 and Bax in after different cell treatments; (b) gray value analysis of Bcl-2, Oct-4, Nanog, DLG2 and Bax by western blot analysis; *(c) protein expression of Bcl-2, Oct-4, Nanog, DLG2 and Bax after different cell treatments; *, $p< 0.05$ compared with the blank and NC groups (p value was obtained by one-way ANOVA and the experiment was repeated three times). miR-23a, microRNA-23a-3p; DLG2, discs large homolog 2; NC, negative control; Bax, Bcl2-associated X protein; Bcl-2, b-cell lymphoma-2; Oct-4, octamer-binding transcription factor 4; OC, ovarian cancer.

blank group and the NC group (all $p > 0.05$). The miR-23a mimic and siRNA-DLG2 groups showed accelerated viability of OC cells and the optical density (OD) values at 48 h, 72 h, and 96 h were significantly increased (all $p < 0.05$). The growth speed of cells in the miR-23a inhibitor group was markedly slower, with lowered OD values at 48 h, 72 h, and 96 h ($p < 0.05$).

Scratch test was applied to examine the cell migration among groups and the results (Figure 6(b,c)) showed that there was no significant difference in migration distance among the blank, NC, and miR-23a inhibitor + siRNA-DLG 2 groups (all $p > 0.05$). However, cell migration ability in the miR-23a mimic and siRNA-DLG2 groups was remarkably enhanced ($p < 0.05$) in contrast to the blank and NC group; while cell migration in miR-23a inhibitor group was significantly reduced ($p < 0.05$).

Transwell invasion assay was performed for the assessment of the invasion ability of cells in each group, and the results (Figure 6(c,d)) showed that there was no noticeable difference in the number of cells invaded from the Transwell apical chamber to the basolateral chamber between the blank group and the NC group ($p > 0.05$). In comparison to the blank and NC groups, the number of cells invaded from the

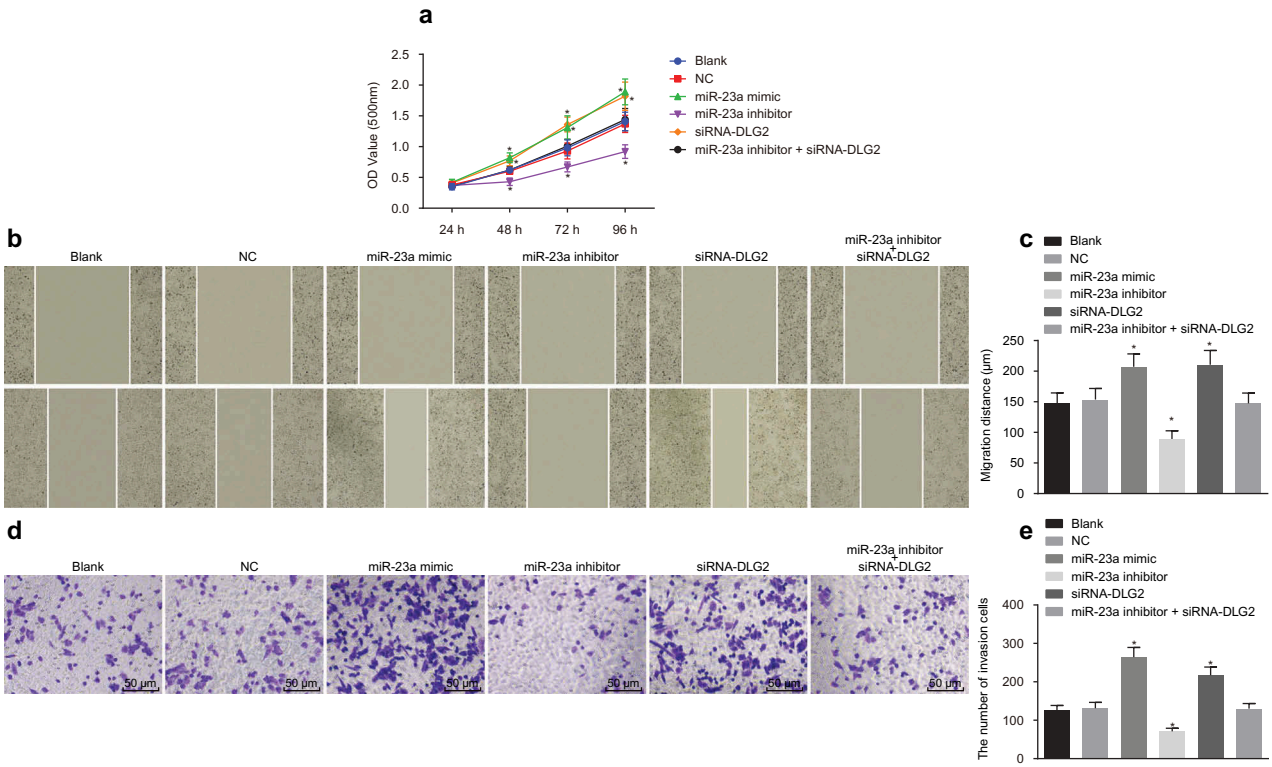

Figure 6. Cell proliferation, migration, and invasion in OC were declined by downregulation of miR-23a. (a) cell proliferation in each group, as detected by CCK-8 assay; (b) cell migration in each group as detected by scratch test; (c) the migration distance of cells in each group under a microscope; (d) the cell invasion assessed by Transwell assay in each group (× 200); (e) the number of invasive cells in each group observed under the microscope; *, $p < 0.05$ compared with the blank group and the NC group (p value was obtained by repeated measures analysis of variance or completely randomized design analysis of variance, and the experiment was repeated three times). miR-23a, microRNA-23a-3p; DLG2, discs large homolog 2; NC, negative control.

Transwell apical chamber to the basolateral chamber in the miR-23a mimic and siRNA-DLG2 groups was dramatically increased, and that in the miR-23a inhibitor group was significantly reduced ($p < 0.05$). There was no distinct difference found regarding the migration ability of the cells in the miR-23a inhibitor + siRNA-DLG2 group compared to the blank and NC group ($p > 0.05$).

Inhibition of miR-23a inhibits cell cycle progression and promotes apoptosis of OC cells

PI single staining was used to further investigate the role of miR-23a in the apoptosis of OC cells. There was no notable difference in cell cycle among the blank, NC and miR-23a inhibitor + siRNA-DLG2 groups ($p > 0.05$) (Figure 7(a,b)). When compared with the blank group and the NC group, the number of cells in G0/G1 phase was decreased in the miR-23a mimic group and the siRNA-DLG2 group, but the cell numbers in the S phase and G2 phase increased. On the contrary, the cells in the G0/G1 phase were increased in the miR-23a inhibitor group, but those in the S phase and G2 phase declined ($p < 0.05$). These results indicated that suppression of miR-23a inhibits the cell cycle progression of OC cells.

Annexin V-Fluorescein isothiocyanate (FITC)/propidium iodide (PI) double staining revealed that there was no significant difference in apoptosis rate among the blank, NC, and miR-23a inhibitor + siRNA-DLG2 groups ($p > 0.05$) (Figure 7(c,d)). In comparison to the blank group and the NC group, the apoptotic rate of the cells in miR-23a mimic group and the siRNA-DLG2 group was markedly decreased but that of the cells in the miR-23a inhibitors group was increased ($p < 0.05$). These results suggested that downregulation of miR-23a promotes the apoptosis of OC cells.

Inhibition of miR-23a accelerates tumor cell sphere formation

The cell sphere formation assay was applied to investigate the change of cell sphere formation in OC cells following transfection. As shown in Figure 8, a cell sphere composed of dozens of cells was observed in the blank group, the NC group, and the miR-23a inhibitor + siRNA-DLG2 group, and the boundary between the cells could not be easily distinguished. The surrounding cells were bright with the central area featuring high cell density and poor transmittance. Compared with the blank and NC groups, cell spheres in the miR-23a mimic and siRNA-DLG2 groups consisted of hundreds of cells, and the new-born single cells were often connected to the cell spheres in a "budding" way; in the miR-23a inhibitor group, a couple of cell spheres formed in suspension, and the cell spheres were small, loose, and "vine-like" with strong refraction and dispersion.

The tumor cell spheres were collected and separated into single cell suspension using trypsin and continued to be subcultured and cultured in SFM. Some cells could continue to

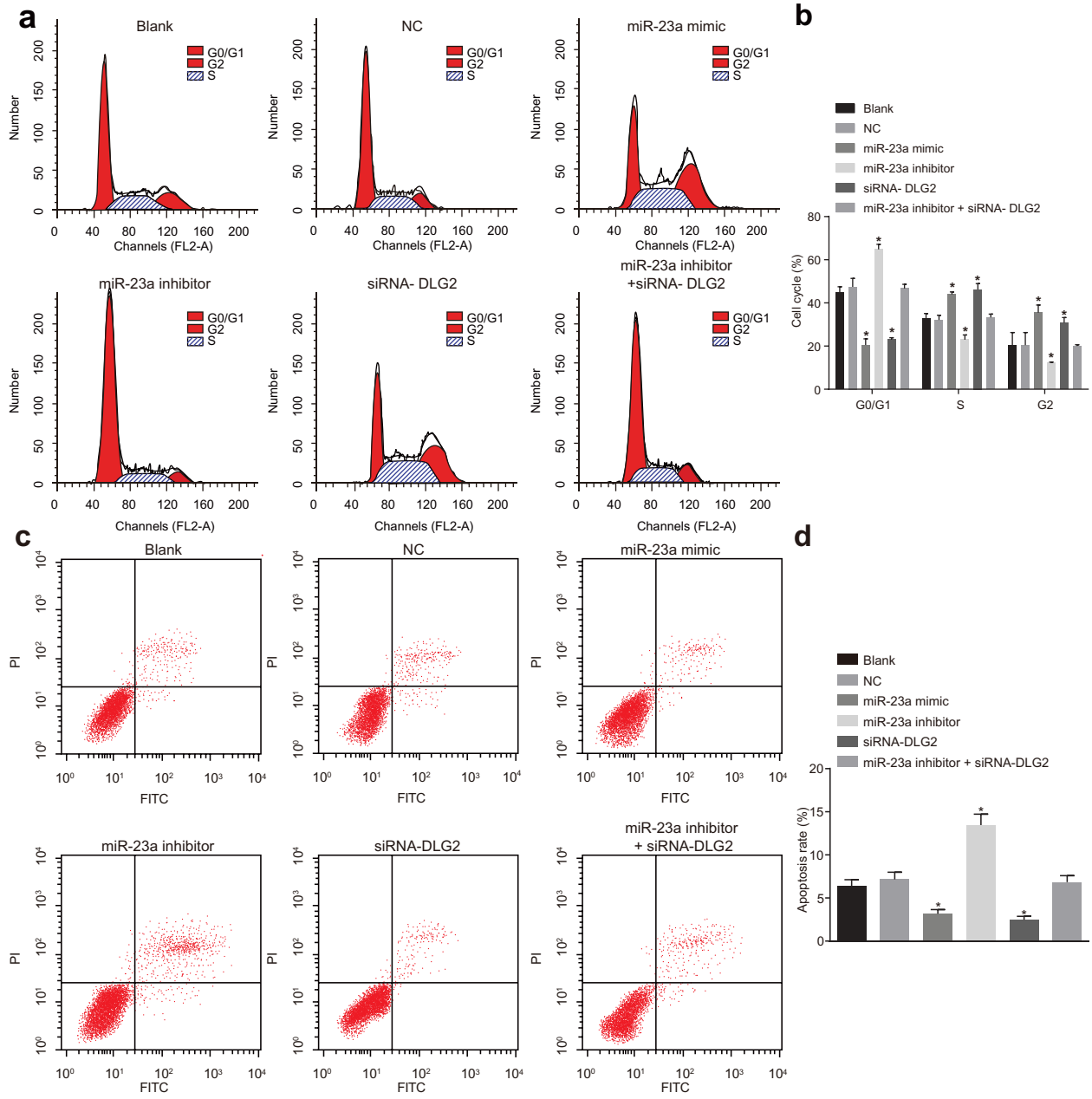

Figure 7. Downregulation of miR-23a promotes the cell cycle arrest and apoptosis of OC cells. (a) cell cycle by PI single staining; (b) cell cycle distribution in each group; (c) cell apoptosis detected by Annexin V-FITC/PI double staining in each group; (d) cell apoptosis rate in each group. *, $p< 0.05$, compared with the blank and NC groups (p value was obtained by ANOVA, and the experiment was repeated three times). miR-23a, microRNA-23a-3p; NC, negative control. OC, ovarian cancer.

proliferate to form new cell spheres floating in SFM. Subculture and amplification were performed every 10 days, and fine colony-forming ability was maintained after 10 subcultures. The SKOV3 cells cultured in SSM were cultivated under SFM conditions. Most of the adherent cells were gradually floated, dead and disintegrated. Only a small fraction of cells survived and formed tumor cell spheres. Under culture conditions at the identical cell density, the number of tumor cell spheres formed in the SFM in the miR-23a mimic and siRNA-DLG2 groups was significantly higher than those found in the blank and NC groups, and the floated cell spheres were gradually increased along with the incubation time. Meanwhile, cell spheres robustly grew with gradual larger volume in a more regular form. After continuous subcultures, the total number of cell spheres was dramatically increased with the colony formation ability maintained. In the miR-23a inhibitor group, the number of tumor cell spheres formed in SFM was significantly reduced compared to the blank and NC groups. After subsequent subcultures, the total number of cell spheres showed a barely noticeable increase. There was no significant difference among the miR-23a inhibitor + siRNA-DLG2, blank, and NC groups ($p > 0.05$).

Inhibition of miR-23a suppresses tumor growth in nude mice

The transfected OC cells were injected into nude mice to observe the tumor formation in order to verify the effect of miR-23a in OC

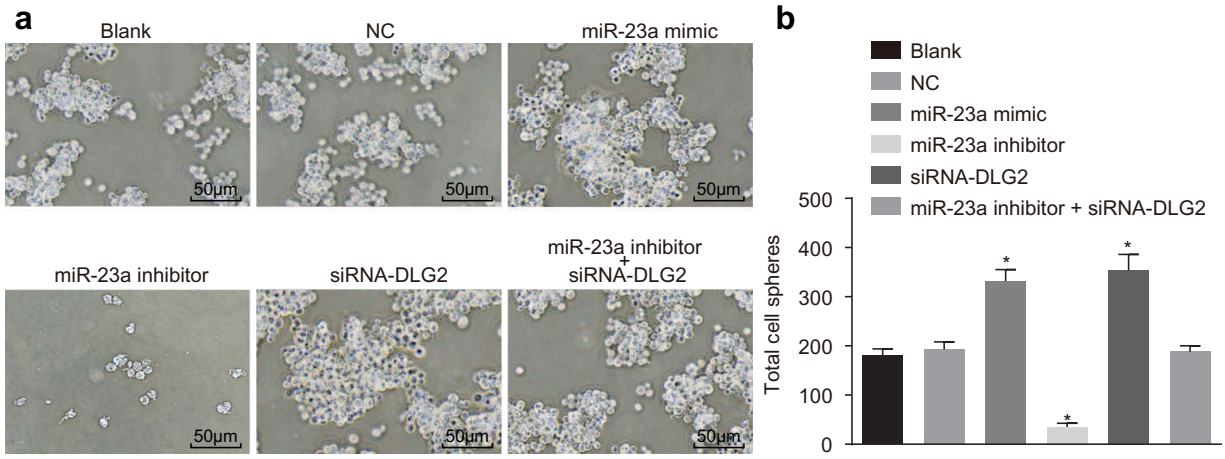

Figure 8. Inhibition of miR-23a enhanced the formation of tumor cell spheres. (a) the sphere forming ability in each group determined using sphere formation assay (× 200); (b) the number of cell spheres after transfection in each group and the data were expressed as mean ± standard deviation and analyzed by one-way analysis of variance. The experiment was repeated three times. miR-23a, microRNA-23a-3p; DLG2, discs large homolog 2; NC, negative control.

cells *in vivo*. There was no notable difference between the blank and NC groups ($p > 0.05$), and similarly, no notable difference was observed between the miR-23a inhibitor + siRNA-DLG2 group ($p > 0.05$). However, the tumor in nude mice of the miR-23a mimic and siRNA-DLG2 groups grew heavier with an increase in time when compared with that in the blank and NC groups ($p < 0.05$) and the tumor volume in the miR-23a inhibitor group was smaller along the time than that in the blank and NC groups ($p < 0.05$) (Figure 9).

Discussion

Accumulating researches have demonstrated that miRNAs are involved in the pathogenesis of tumors such as OC, due to their function as regulators in cancer occurrence and development.[17,18] Prior to conducting this experiment, we did our own research trying to accumulate some evidence on what role miRNAs play in OC, more specifically, the involvement of miR-23a and DLG2 in OC. A list of evidence

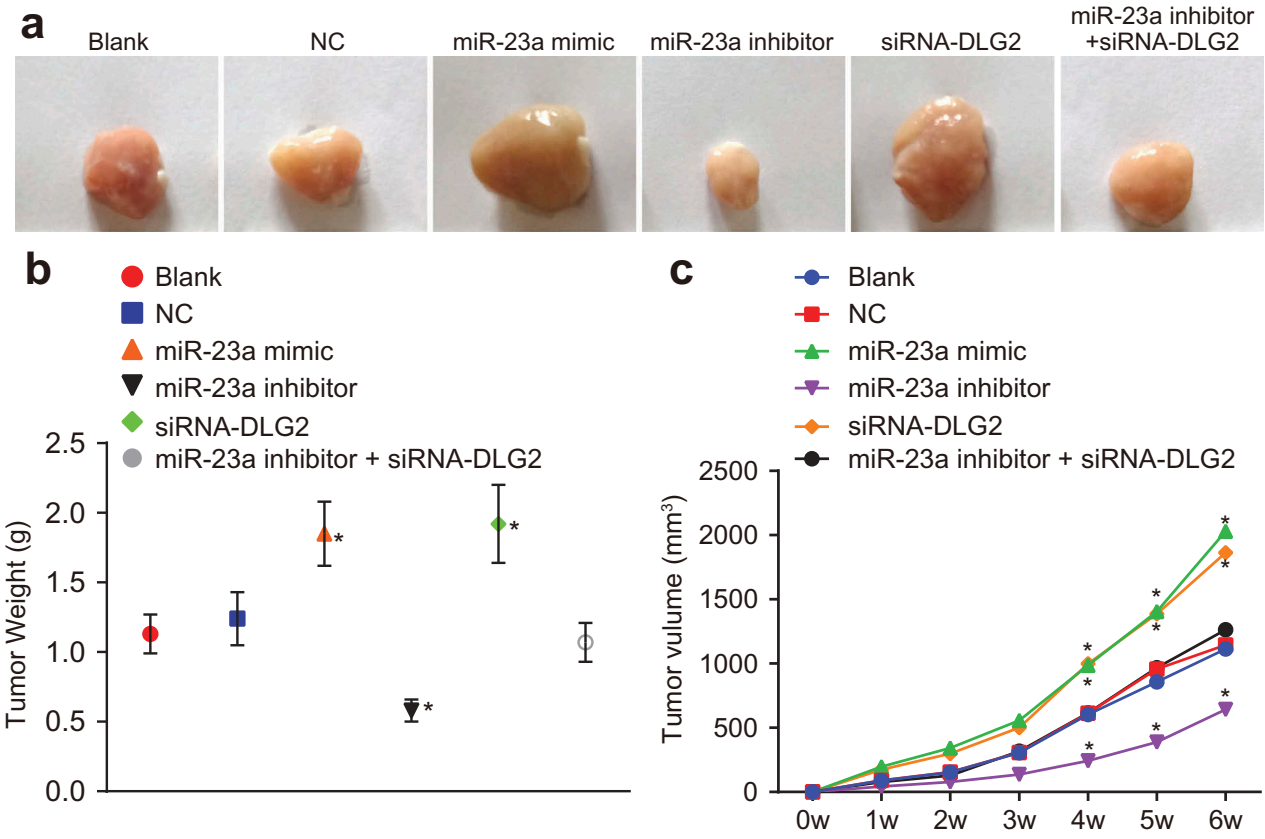

Figure 9. Suppression of miR-23a inhibits tumor growth in nude mice. (a) the size of nude mice transplanted tumors after transfection. (b) the weight of nude mice transplanted tumors after transfection. (c) changes in the volume of nude mice transplanted tumors after transfection with time prolonged. *, $p < 0.05$ compared with the blank group and NC group (p value was obtained by repeated measures analysis of variance, n = 5). miR-23a, microRNA-23a-3p; NC, negative control.

from both cancer tissues and cell lines that were generated in this study demonstrated that downregulation of miR-23a promotes cell apoptosis and inhibits the cancer stem cell formation, increasing their cloning and self-renewal capacities of OC stem cells by targeting DLG2, thus dampening the occurrence and development of OC (Figure 10).

At the beginning of this study, prediction platforms provided a miRNA candidate miR-23a, which was found to be highly expressed in OC, while there was a low expression in its potential target DLG2 in OC. Similarly, a previous study has revealed that miR-23a was highly expressed in gastric cancer tissues and cell lines.[19] According to the examination, highly expressed miR-23a in cancers of the digestive system was associated with a poor prognosis.[20] Another study demonstrated that OC tissues had a high miR-23a expression, which was consistent with our findings.[21] In addition, DLG2 was found to be downregulated in oropharyngeal squamous cell carcinoma.[22] Supported by dual-luciferase reporter gene assay, it confirmed that miR-23a could specifically bind to DLG2 gene and inhibit its expression. Furthermore, we observed that the mRNA and protein expression of Bcl-2, Oct-4 and Nanog was decreased while DLG2, Bax mRNA, and protein expression was increased when miR-23a was inhibited in OC cells. Bcl-2 is known to be a member of anti-apoptotic proteins, while Bax, a member of pro-apoptotic proteins, belonging to the Bcl-2 family.[23] Bcl-2 and Bax were confirmed to be related to the chemotherapy resistance in various tumors.[24] In our study, miR-23a inhibition was shown to suppress Bcl-2 expression but increase Bax expression, which was indicative of an accelerated OC cell apoptosis. Meanwhile, Oct-4, Nanog, and CD133 are known as stem cell markers and indicated as invasive and predictive markers in relation to a poor prognosis in oral squamous cell carcinoma (OSCC).[25] In addition, Oct4 and Nanog possess oncogenic properties, and are highly expressed in OC cell lines due to regained self-renewal ability in the tumor microenvironment.[26] Hence, Oct-4 and Nanog downregulation triggered by miR-23a inhibition indicate that the miR-23a inhibition correlates with a suppressive role in self-renewal ability.

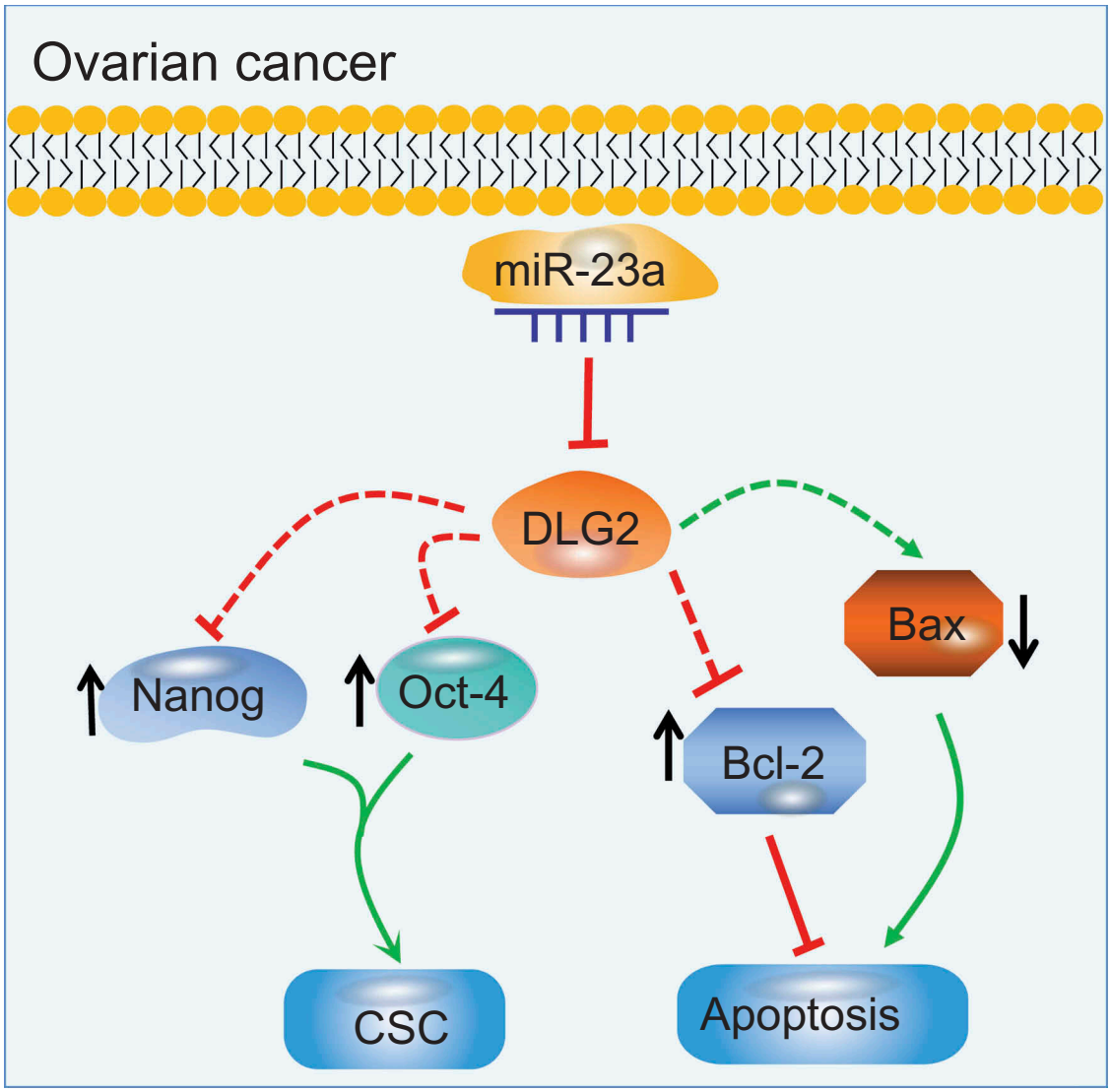

Figure 10. MiR-23a inhibits OC cell apoptosis and promotes the formation of tumor stem cells. Functionally, miR-23a suppresses the expression of DLG2, by which to elevate the expression of anti-apoptotic protein Bcl-2 and stem cell markers Oct-4 and Nanog, and to suppress the expression of the pro-apoptotic protein Bax, thereby repressing OC cell apoptosis and inducing the formation of tumor stem cells. miR-23a, microRNA-23a-3p; DLG2, discs large homolog 2; Bax, Bcl2-associated X protein; Bcl-2, b-cell lymphoma-2; Oct-4, octamer-binding transcription factor 4; CSC, cancer stem cell. OC, ovarian cancer.

In addition, the proliferation, migration, invasion, cloning and self-renewal abilities of OC cells were also observed and were found to be significantly decreased upon miR-23a inhibition, along with the tumor volumes in nude mice, while the apoptosis ability was increased. Several miRNAs have been identified to be at a high level in OC, such as miR-222 and miR-182, and their inhibition also suppresses cell invasion and metastasis in human OC.[27,28] Previous researches have demonstrated that aberrant expression of miR-23a can be found in patients with human diseases or cancers, and this miRNA regulates proliferation, apoptosis, metastasis, and invasion of tumors.[29,30] The high expression of miR-23a is closely associated with the occurrence and development of OC.[21] Another study reported that the reduced expression of miR-23a enhanced the apoptosis rate of the OC A2780 cell lines.[31] Based on various evidence listed above, there is no doubt that inhibition of miR-23a has a suppressive effect on OC progression. Specific interaction between DLG2 and miR-23a was verified by introducing DLG2 silencing plus miR-23a inhibition into OC cells, and as a consequence, we found that DLG2 silencing resulted in the elimination of the suppressive effect of miR-23a inhibition in terms of OC progression. DLG2 has been reported to have the ability to inhibit the progression of tumors in oropharyngeal squamous cell carcinomas (OSCCs).[32] Our study also found that OC oncogenesis could be inhibited by the upregulation of DLG2 induced by miR-23a depletion.

In conclusion, the current study suggests that miR-23a suppression inhibits the progression of OC via upregulation of DLG2, which could result in the inhibition of proliferation, invasion, and migration but increased apoptosis of OC. These findings may open novel avenues for future OC therapies, although more in-depth understanding is required for the various roles of miR-23a in OC stem cells.

Material and methods

Ethics statement

All experiments were conducted under the guidelines and principles of the Declaration of Helsinki. The experimental program was approved by the Ethics committee of The Second Affiliated Hospital of Harbin Medical University. All study subjects have signed written informed consent prior to the experiment. Meanwhile, all experimental operations followed the International Convention on Laboratory Animal Ethics and complied with relevant national regulations. All efforts were made to minimize animal suffering.

Microarray-based gene expression analysis and miRNA prediction

The GSE14407 and GSE38666 expression matrix and probe annotation files with OC tissues and normal tissues were downloaded from the GEO database (https://www.ncbi.nlm.nih.gov/geo/). The gene annotation platforms for annotating GSE14407 and GSE38666 were GPL570-[HG-U133_Plus_2] Affymetrix Human Genome U133 Plus 2.0 Array. In addition, R language "affy" package was applied for background correction and standardized preprocessing on gene expression data. The "limma" package was used for DEG screening. The corrected *p* value was represented as *adj.P.Val*. Those genes conformed to *adj.P.Val* <0.05 and |LogFoldChange| >2 were considered as DEGs, based on which, the heatmap was plotted. The DigSee disease gene search engine (http://210.107.182.61/geneSearch/) was used to search abstracts on MEDLINE to find the relation between the gene and the disease,[33] which was used to retrieve OC-related genes. OC disease genes and DEGs were input into the String database (https://string-db.org/) for gene–gene interaction and KEGG enrichment analysis. The visualization of gene–gene interactions was performed using Cytoscape 3.6.0 software. MiRDB (http://www.mirdb.org/), DIANA (http://diana.imis.athena-innovation.gr/DianaTools/index.php?r=microT_CDS/index), miRWalk (http://mirwalk.umm.uni-heidelberg.de/), mirDIP (http://ophid.utoronto.ca/mirDIP/), TargetScan (http://www.targetscan.org/vert_71/) and microRNA (http://34.236.212.39/microrna/getGeneForm.do) were employed to predict the miRNAs that could regulate DEGs. The difference between the DEGs of two gene chips or the difference among six miRNA prediction results was compared using jvenn (http://jvenn.toulouse.inra.fr/app/example.html).

Study subjects

From January 2015 to December 2016, 50 patients (between the ages of 21 to 79 years, with the mean age of 48.22 ± 2.95 years) that were clinically and pathologically diagnosed with OC in The Second Affiliated Hospital of Harbin Medical University were enrolled in the experiment. All cases were diagnosed at grade II OC[34] and the enrolled subjects were confirmed with OC by clinical, imaging, and pathological diagnosis. All patients received standard medical diagnosis and treatment. None of the patients had received any radiotherapy or chemotherapy treatments before experiments. Patients with secondary lesions failed to follow standard diagnosis and treatment or had a history of other malignancies were excluded. OC and adjacent normal tissues were collected from OC patients, out of which 50 OC tissues were classified as OC group and 20 adjacent normal tissues were used as a control. All tissue samples were preserved in a refrigerator at −80°C.

Immunohistochemistry

Formalin (10%)-fixed and paraffin-embedded tissue samples were sliced into 4 μm serial sections and baked at 60°C for 1 h, followed by deparaffinization with xylene and dehydration with gradient alcohol. Subsequently, samples were subjected to antigen retrieval using sodium citrate (0.1 M), boiled for 20 min, cooled to room temperature and rewashed with 0.2 mol/L phosphate-buffered saline (PBS) three times (5 min each), and finally inactivated in 3% catalase for 15 min. The sections were then rinsed with 0.2 mol/L PBS (pH 7.4) three times (5 min each) and dried. Samples were blocked with 5% bovine serum albumin (BSA) at 37°C for 30 min and incubated with rabbit anti-DLG2 polyclonal antibody (1: 400, ab50316, Abcam Inc., Cambridge, MA, USA) at 4°C overnight. After washing the samples in 0.2 mol/L PBS (pH 7.4) (3 × 5 min)

and drying, biotinylated goat anti-rabbit immunoglobulin G (IgG) (1: 2000, ab6721, Abcam Inc., Cambridge, MA, USA) was added to the samples for incubation at 37°C for 30 min. Meanwhile, chromogenic reagent was prepared, and a drop of A, B, C solution of diaminobenzidine (DAB) (DA1010, Beijing Solarbio Science & Technology Co., Ltd., Beijing, China) was added into the sections with additional 1 mL distilled water, respectively. All solutions were mixed completely and stored at 4°C before use. Sections were rewashed in 0.2 mol/L PBS (pH7.4) three times, 5 min each and then placed under dark conditions at room temperature for 8 min and washed again with running water. Subsequently, sections were stained with hematoxylin, dehydrated, cleared and sealed. The stained sections were observed and photographed under the light microscope (XSP-36, Shenzhen Bo as Optical Instruments Co., Ltd., Shenzhen, China). Five high-magnification fields (× 200) were selected randomly for each section, with 100 cells per field. If positive cells < 5%, then the output was considered as negative and if positive cells ≥ 5%, then it was considered as positive.[35] The immunohistochemical results were scored by two individuals independently using a double-blind method.

RT-qPCR

Total RNA was extracted using RNA extraction kit (10296010, Invitrogen Inc., Shanghai, China). After RNA concentration and purity were identified, RNA was reversely transcribed into cDNA using PrimeScript RT Kit (RR014A, Takara Biotechnology Company, Beijing, China). The reverse transcription system was conducted using 10 μL reaction volume, and the reaction conditions were as follows: reverse transcription took place at 37°C (15 min × 3 times), followed by inactivation at 85°C for 5 s. Primers of miR-23a, DLG2, Bax, Bcl-2, Oct-4, Nanog, internal reference U6 and glyceraldehyde 3-phosphate dehydrogenase (GAPDH) were designed and synthesized by TAKARA Company (Kyoto, Japan) (Table 1). RT-qPCR was performed according to the PCR kit (KR011A1, Tiangen Biotechnology Co., Ltd., Beijing, China). The reaction conditions were as follows: pre-denaturation at 95°C for 5 min; 30 cycles of denaturation at 95°C for 40 s, annealing at 57°C for 40 s, extension at 72°C for 40 s; extension at 72°C for another 10 min, and at 4°C for 5 min. The reaction system consisted of 10 μL SYBR Premix Ex TaqTM II, 0.4 μL PCR Forward Primer (10 μM), 0.4 μL PCR Reverse Primer (10 μM), 2 μL DNA template and 7.2 μL sterile distilled water. The relative expression level of miR-23a was calculated using U6 as an internal reference and the expression levels of DLG2, Bax, Bcl-2, Oct-4, and Nanog were calculated using GAPDH as an internal reference. $2^{-\triangle\triangle Ct}$ method was used to determine and compare the gene expression levels in each group. The experiment was repeated three times.

Table 1. RT-qPCR primer sequence.

Gene	Primer sequence
Mir-23a	F: 5′- GGGGATCACATTGCCAGG-3′ R: 5′- AGTGCGTGTCGTGGAGTC-3′
DLG2	F: 5′-GATGACCCTGGCATATTTATTACGA-3′ R: 5′-ACGATAGACCCTGCTTCCTTCA-3′
Bax	F: 5′- CGAGTGGCAGTGACATGT-3′ R: 5′- TCTTCTTCCAGATGGTGAG-3′
Bcl-2	F: 5′-CCGAGATGTCCAGCCAGCT-3′ R: 5′-CAGTTCCACAAAGGCATCC-3′
Oct-4	F: 5′-AAGCTGCTGAAACAGAAGAGG-3′ R: 5′-ACACGGTTCTCAATGCTAGTC-3′
Nanog	F: 5′-ATTTGCGGCCGCATGAGTGTGGGTCTTC-3′ R: 5′-CGGGATCCTCATATTTCACCTGGTGGAG-3′
GAPDH	F: 5′-GGAAGGTGAAGGTCGGAGTC-3′ R: 5′-GACCACCTGGTGCTCAGTGT-3′
U6	F: 5′-GCTTCGGCAGCACATATACTAAAAT-3′ R: 5′-CGCTTCACGAATTTGCGTGTCAT-3′

Note: F, forward; R, reverse; miR-23a, miRNA-23a; DLG2, discs large homolog 2; Bax, Bcl2-associated X protein; Bcl-2, B-cell lymphoma-2; Oct-4, octamer-binding transcription factor 4; GAPDH, glyceraldehyde 3-phosphate dehydrogenase; RT-qPCR, reverse transcription quantitative polymerase chain reaction.

Western blot analysis

Total protein was extracted using a radioimmunoprecipitation assay (RIPA) kit (R0010, Beijing Solarbio Science & Technology Co. Ltd., Beijing, China). The total protein concentration was estimated using a bicinchoninic acid (BCA) protein detection kit. After the determination of protein concentration, proteins were separated by polyacrylamide gel electrophoresis and then transferred onto nitrocellulose membranes by the wet-transfer method. Subsequently, the membranes were blocked with 5% BSA for 1 h and then incubated overnight at 4°C with diluted primary rabbit-anti polyclonal antibodies to DLG2 (1: 400, ab2930), Bax (1: 500, ab53154), Bcl-2 (1: 500, ab59348), Oct-4 (1: 500, ab18976), Nanog (1: 200, ab2124) and GAPDH (1: 2500, ab9485), which were all purchased from Abcam (Cambridge, MA, USA). After washing with PBS (5 min × 5 times), the membranes were incubated with horseradish peroxidase (HRP)-labeled goat anti-rabbit immunoglobulin G (IgG) antibody (1: 5000, Beijing Zhongshan Biotechnology Co., Ltd., Beijing, China), and then washed 3 times with tris-buffered saline Tween (Tween 20) (TBST) (5 min/each). Finally, membranes were developed in the dark using the electrogenerated chemiluminescence (ECL) reagent (WBKLS0500, Pierce, Rockford, IL, USA), observed and imaged. The gray value ratio of the target protein to the internal reference was used as the relative protein expression.

Cell grouping and transfection

Human OC cell line SKOV3 obtained from Cell Bank of the Chinese Academy of Sciences (Shanghai, China) were inoculated in a six-well plate (1×10^5 cells per well) with Dulbecco modified Eagles Medium (DMEM, 190040, GIBCO BRL, Grand Island, NY, USA) that contained 10% fetal bovine serum (FBS) under saturated humidity at 37°C with 5% CO_2. Once SKOV3 cells reached 80–90% confluence, the cells were sub-cultured with DMEM containing 10% FBS.

Cells in logarithmic growth phase were assigned into six groups: 1) blank, 2) NC, 3) miR-23a mimic, 4) miR-23a inhibitor, 5) siRNA-DLG2, and 6) miR-23a inhibitor + siRNA-DLG2 groups. The cells were then inoculated in a six-well plate 24 h before transfection. When the cells reached 30–50% confluence, the cells were transfected using lipofectamine 2000 (11668–019, Invitrogen Inc., Carlsbad, CA, USA). Plasmids (NC, miR-23a mimic, miR-23a inhibitor, siRNA-DLG2, and miR-93 inhibitor + siRNA-DLG2, 100 pmol each) were diluted in 250 μL serum-free Opti-MEM

(51985042, GIBCO BRL, Grand Island, NY, USA) to a final concentration of 50 nM and incubated at room temperature for 5 min. Meanwhile, 5 μL of lipofectamine 2000 was also diluted in 250 μL serum-free Opti-MEM and incubated at room temperature for 5 min. When both plasmid and lipofectamine solution were diluted, they were mixed and incubated at room temperature for 20 min after which they were added to cell cultures. Cells were incubated with plasmid-lipofectamine mixture under saturated humidity at 37°C with 5% CO_2 for 6–8 h, and then cultured in complete medium for 24–48 h after which further experiments were conducted.

OC cell culture

SKOV3 cells that were cultured in serum-supplemented medium (SSM) (DMEM containing 10% FBS) and in good growth condition were used to prepare cell suspension using conventional method, and then centrifuged at 179 × g for 5 min to remove the supernatant. After being washed twice in 0.01 M PBS, the cells were re-suspended in serum-free medium (SFM) (DMEM/F12 [1: 1, HyClone Company, Logan, UT, USA], and supplemented with 0.4% BSA [Sigma-Aldrich Chemical Company, St Louis, MO, USA]). Subsequently, the cells were mixed with epidermal growth factor (EGF) (20 ng/mL, PeproTech, Rocky Hill, NJ, USA), basic fibroblast growth factor (bFGF) (10 ng/mL, PeproTech, Rocky Hill, NJ, USA), insulin (5 μg/mL) and the mixture were sterilized by filtration and kept at 4°C prior to being utilized. The cells were inoculated into new culture bottles with a cell density of 2×10^5 cells/mL, in a 5% CO_2 incubator at 37°C. In addition to complete culture medium, the cell cultures were provided with a supplement of 0.25 mL serum-free medium every other day. Different from the conventional medium replacement that only added with fresh SFM, the original culture medium was not absorbed in order to avoid the loss of cell spheres.

Magnetic activated cell sorting

CD133 positive cells were sorted using magnetic activated cell sorting kit and corresponding instrument strictly according to the instructions when floating cell spheres were observed to have 150–200 μm in diameter. Cells that met the diameter criteria were collected and mixed with the immunomagnetic bead cell sorting solution at a density of 200 μL/10^8 cells. Single cell suspension was prepared by trituration, and then cells were mixed with the CD133 antibody conjugated to micromagnetic beads (100 μL/10^8 cells). After incubation at 4°C for 30 min, the cells were washed with sorting solution (1 mL/10^8 cells), and the supernatant was discarded after centrifugation. The cells were collected and re-suspended with sorting solution (500 μL/10^8 cells) before being added to the separation column. In the end, 2 mL separation solution was added to elute CD133 positive cells.

Flow cytometry was used to verify the sorting efficiency. The sorted CD133 positive cells were assigned to the homotypic control group, pre-sorting group, and post-sorting group. In the homotypic control group, 5 μL allophycocyanin (APC) labeled IgG antibody and 95 μL PBS were added. While in the pre-sorting and post-sorting groups, 5 μL APC-labeled anti-CD133/2 antibody and 95 μL PBS were added to the cells and incubated at 37°C for 30 min. After being washed with PBS, centrifugation was carried out to remove the supernatant. A total of 100 μL PBS solution was used for the resuspension of the cells before flow cytometry.

Immunofluorescence assay

CD133 expression in OC stem-like cells with or without gel layer was detected by immunofluorescence assay. The cells were incubated with 5% CO_2 at 37°C for 6 h and then fixed with 40 g/L paraformaldehyde and 1% glutaraldehyde. After sealing, cells were incubated with CD133 antibody overnight and then subjected to secondary antibody with the avoidance of light for 30 min. Subsequently, the nucleus was stained by 4′, 6-diamidino-2-phenylindole (DAPI) and the nucleation was observed using the laser scanning confocal microscope before being sealed and fixed.

Dual-luciferase reporter gene assay

MicroRNA.org was used to predict the target genes of miR-23a, and the dual-luciferase reporter gene assay was used to determine whether DLG2 was a direct target of miR-23a or not. The synthesized gene segment of DLG2-3′-untranslated region (3′UTR) was introduced into the reporter vector pMIR-reporter (Promega, Madison, WI, USA) through the endonuclease sites of Sal I and Bgl II. The complementary sequence mutation sites of seed sequences were designed based on the wild-type DLG2. After restriction endonuclease digestion, the target segment was inserted into pMIR-reporter vector using the T4 DNA ligase. After identification of positive clones, the recombinant plasmid was verified by DNA sequencing, cloned into psiCHECK-2 vector, and then transformed into *Escherichia coli* DH5α. After *E. coli* inoculation, the plasmids were extracted using Plasmid Mini Kit (Omega Bio-Tek, Norcross, GA, USA). Meanwhile, cells were seeded in a six-well plate (1×10^4 cells per well), transfected after cell adherence, cultured for 48 h, and collected for the luciferase activity measurement. The change of luciferase activity of DLG2 3′-UTR that induced by miR-23a in cells was measured using a dual-luciferase assay kit (Genecopoeia Inc., Rockville, MD, USA). Luminance intensity was detected by a Glomax 20/20 luminometer (Promega, Madison, Wisconsin, USA). The experiments were repeated three times.

Cell counting kit-8 (CCK-8) assay

The transfected human OC cells were paved on a 96-well plate and 100 μL cell culture medium was added to each well to obtain the cell density at 2×10^3 cells/mL. The plate was incubated at 37°C and cell viability was measured at 24, 48, and 72 h after incubation. Cells in each well were incubated with 10 μL CCK-8 reagent (C0037, Beyotime Institute of Biotechnology, Shanghai, China) at 37°C for 2 h before detection on a microplate reader (Multiskan FC, Thermo Fisher Scientific Inc., Waltham, MA, USA). The OD value was detected at a wavelength of 450 nm/

630 nm. For detection, three parallel wells were set for each group to get the average value. The experiment was repeated three times, and the cell viability curve was plotted using time point as abscissa and the OD value as ordinate.

Scratch test

After 24-h transfection, cells in good growth condition were seeded in a six-well plate (1×10^6 cells per well). When cell confluence reached about 95%, vertical linear scratches were made by a sterile 200 μL pipette tip. Scratched cells were then rinsed with D-Hanks solution, and the plate was cultured with the addition of serum-free medium. Images of the scratches were acquired at 0 h and 48 h. Image-Pro Plus Analysis software (Media Cybernetics, Silver Spring, MD, USA) was used to measure cell migration distance. The experiment was conducted three times to obtain average values.

Transwell assay

After transfection for 72 h, the cells were starved in serum-free medium for 12 h and then detached to avoid effects of serum. Cells were rinsed twice in PBS and re-suspended using serum-free medium Opti-MEMI (31985–070, Invitrogen Inc., Carlsbad, CA, USA) containing 10 g/L BSA and cell concentration was adjusted to 2×10^6 cells/mL. The experiments were performed using a 24-well Transwell chamber (8 μm-pore-size; 3413, Corning, New York, USA) with 3 chambers per group. A total of 50 μL Matrigel (40111ES08, Sigma-Aldrich Chemical Company, St Louis, MO, USA) was placed in the chamber before the experiment. After 48 h, 200 μL (4×10^4 cells) single cell suspension solution was added into the apical chamber, while the basolateral chamber was added with 650 μL Opti-MEMI (31985–070, Invitrogen Inc., Carlsbad, CA, USA) containing 10% FBS and placed in a 5% CO_2 incubator at 37°C for 12 h. The Transwell chambers were taken out and washed with PBS and fixed in methanol solution for 30 min at room temperature, then stained with 0.1% crystal violet for 20 min. The upper layer cells of the microporous membrane were carefully erased with cotton swabs, and the images were observed and recorded under an inverted optical microscope. Four fields were randomly selected to calculate the number of cells passing through the microporous membrane to obtain the average value. The experiment was repeated three times.

Flow cytometry

Cells were harvested 72 h after transfection and treated with 0.25% trypsin to adjust the cell density to 1×10^6 cells/mL. Next, 1 mL of cells was centrifuged at 403 × g for 10 min, after which the supernatants were discarded. The cells were then collected and re-suspended with 2 mL PBS and centrifuged to discard supernatant. The cells were fixed with pre-cooled 70% ethanol solution and incubated at 4°C overnight, which were washed on the next day twice with PBS. Subsequently, 100 μL cell suspension was mixed with 50 μg PI containing RNAase, followed by incubation under dark conditions for 30 min and filtering with a 300-mesh nylon mesh. Finally, red fluorescence was measured at an excitation wavelength of 488 nm to detect the cell cycle using flow cytometer (BD, Biosciences, Franklin Lakes, NJ, USA).

Apoptosis was detected by FITC/PI double staining. The treated cells were collected 48 h after incubation at 37°C with 5% CO_2, followed by two PBS washes. After centrifugation, the cells were resuspended in 200 μL binding buffer. Subsequently, 10 μL Annexin V-FITC (ab14085, Abcam, Cambridge, MA, USA) and 5 μL PI were mixed gently with the cells, and the mixture stood at room temperature for 15 min avoiding exposure to light, followed by the addition of 300 μL binding buffer. Finally, apoptosis was detected with flow cytometer at an excitation wavelength of 488 nm.

Sphere formation assay

High glucose DMEM containing 10% FBS was added to the amplified OC cells for *in vitro* culture in an incubator with 5% CO_2 at 37°C. When the cell confluence reached 80%, they were harvested after trypsinization by 0.25% trypsin, and then resuspended in the stem cell conditioned medium after the supernatant was discarded. Cells were then inoculated on a six-well ultra-low-attachment plate (with a density of no more than 1000 cells/well) with the conditions of 5% CO_2 at 37°C. After 6-day incubation, when the tumor sphere grew to a size of 50 μm, the cell suspension was collected and centrifuged at a low speed of 64 × g for 5 min to separate the tumor spheres and single cells. The tumor spheres were precipitated at the bottom of the centrifuge tube, and the smaller single cells remained suspended in the supernatant, which was removed, and the cell pellet was resuspended with PBS. This step was repeated twice to obtain purer sphere-forming cells. The collected pure sphere-forming cells were incubated with 0.25% trypsin/0.02% ethylenediaminetetraacetic acid (EDTA) in an incubator at 37°C for 2 min and then dispersed into individual cells by trituration. A total of 5 mL PBS was added to the cells, and the cell suspension was centrifuged at 18°C at 179 × g for 5 min to remove the supernatant. The cells were washed twice with PBS, and the digestive enzymes were removed, and then cells were resuspended with stem cell conditioned medium. The cells were counted 3 times to obtain the average number of cells. Finally, the cells (1000 cells/well) were re-inoculated into a six-well ultra-low-attachment plate (BD Biosciences, Franklin Lakes, NJ, USA) and cultured in a 5% CO_2 incubator at 37°C.

Tumorigenicity in nude mice

Thirty female athymic nude mice (5–6 weeks) were purchased and raised by the Animal Experimental Center of The Second Affiliated Hospital of Harbin Medical University. Nude mice were raised at a constant temperature (25–27°C) and constant humidity (45–50%). After transfection, once the cells reached 80–90% confluence, they were detached before centrifugation, washed with PBS 2–3 times, resuspended and counted. The cell density was adjusted to 1×10^7 cells/mL, and 20 μL cell suspension was inoculated into the subcutaneous axilla of nude mice. Five mice were inoculated in each group. After 6

weeks, the nude mice were sacrificed with CO_2. The size of the transplanted tumors was measured for pathological examination. The growth curve was drawn with the volume records of transplanted tumors, using the following formula: $(a \times b^2)/2$ (a represents the longest diameter of the tumor and b is the shortest diameter of the tumor).

Statistical analysis

All data were processed by SPSS 21.0 statistical software (IBM, Corp, Armonk, NY, USA). The measurement data were expressed by mean ± standard deviation. The *t*-test was used to compare data between two groups. One-way analysis of variance (ANOVA) was used for comparisons among multiple groups. $p < 0.05$ indicated a significant statistical difference.

Abbreviations

OC:	Ovarian cancer
Mirnas:	MicroRNAs
OS:	Osteosarcoma
DLG:	Discs large homolog 2
DEG:	Differentially expressed gene
HE:	Hematoxylin-eosin
MIA:	Morphological image analysis
PBS:	Phosphate buffered saline
BSA:	Bovine serum albumin
IgG:	Immunoglobulin G
DAB:	Diaminobenzidine
RT-qPCR:	Reverse transcription quantitative polymerase chain reaction
BCA:	Bicinchoninic acid
HRP:	Horseradish peroxidase
TBST:	Tris-buffered saline Tween
ECL:	Electrogenerated chemiluminescence
NC:	Negative control
SSM:	Serum-supplemented medium
SFM:	Serum-free medium
bFGF:	Basic fibroblast growth factor
APC:	Allophycocyanin
CCK:	Cell counting kit-8
OD:	Optical density
PI:	Propidium iodide
ANOVA:	Analysis of variance

Acknowledgments

We would like to show our sincere gratitude to the reviewers for their valuable comments.

Disclosure of Potential Conflicts of Interest

No potential conflicts of interest were disclosed.

Funding

This study was supported by Heilongjiang Health Department Research Project [No. 13145] and Education Department of Heilongjiang Province Research Project (No.12541373).

Competing interest

The authors declare that they have no competing interests.

References

1. Tsunoda AT, Ribeiro R, Reis RJ, Da Cunha Andrade C, Marques RM, Baiocchi G, Fin F, Zanvettor PH, Falcao D, Batista TP, et al. Surgery in ovarian cancer - Brazilian Society of Surgical Oncology consensus. BJOG. 2018. PubMed: 29900651. doi:10.1111/1471-0528.15328.
2. Grzelak MM, Wrobel PM, Lankosz M, Stegowski Z, Chmura L, Adamek D, Hesse B, Castillo-Michel H. Diagnosis of ovarian tumour tissues by SR-FTIR spectroscopy: a pilot study. Spectrochim Acta A Mol Biomol Spectrosc. 2018;203:48–55. PubMed: 29859492. doi:10.1016/j.saa.2018.05.070.
3. Ghoneum A, Afify H, Salih Z, Kelly M, Said N. Role of tumor microenvironment in ovarian cancer pathobiology. Oncotarget. 2018;9(32):22832–22849. PubMed: 29854318. doi:10.18632/oncotarget.25126.
4. Worzfeld T, Pogge von Strandmann E, Huber M, Adhikary T, Wagner U, Reinartz S, Muller R. The unique molecular and cellular microenvironment of ovarian cancer. Front Oncol. 2017;7:24. PubMed: 28275576. doi:10.3389/fonc.2017.00024.
5. Langhe R. microRNA and Ovarian Cancer. Adv Exp Med Biol. 2015;889:119–151. PubMed: 26659000. doi:10.1007/978-3-319-23730-5_8.
6. Gomez-Raposo C, Mendiola M, Barriuso J, Hardisson D, Redondo A. Molecular characterization of ovarian cancer by gene-expression profiling. Gynecol Oncol. 2010;118(1):88–92. PubMed: 20439111. doi:10.1016/j.ygyno.2010.03.012.
7. Lovat F, Valeri N, Croce CM. MicroRNAs in the pathogenesis of cancer. Semin Oncol. 2011;38(6):724–733. PubMed: 22082758. doi:10.1053/j.seminoncol.2011.08.006.
8. Iwasaki T, Tanaka K, Kawano M, Itonaga I, Tsumura H. Tumor-suppressive microRNA-let-7a inhibits cell proliferation via targeting of E2F2 in osteosarcoma cells. Int J Oncol. 2015;46(4):1543–1550. PubMed: 25647078. doi:10.3892/ijo.2015.2867.
9. Pan Z, Shan Q, Gu P, Wang XM, Tai LW, Sun M, Luo X, Sun L, Cheung CW. miRNA-23a/CXCR4 regulates neuropathic pain via directly targeting TXNIP/NLRP3 inflammasome axis. J Neuroinflammation. 2018;15(1):29. PubMed: 29386025. doi:10.1186/s12974-018-1220-7.
10. Jahid S, Sun J, Edwards RA, Dizon D, Panarelli NC, Milsom JW, Sikandar SS, Gumus ZH, Lipkin SM. miR-23a promotes the transition from indolent to invasive colorectal cancer. Cancer Discov. 2012;2(6):540–553. PubMed: 22628407. doi:10.1158/2159-8290.CD-11-0267.
11. Yang Z, Wang XL, Bai R, Liu WY, Li X, Liu M, Tang H. miR-23a promotes IKKalpha expression but suppresses ST7L expression to contribute to the malignancy of epithelial ovarian cancer cells. Br J Cancer. 2016;115(6):731–740. PubMed: 27537390. doi:10.1038/bjc.2016.244.
12. Wu HC, Chen CM, Chen YC, Fung HC, Chang KH, Wu YR. DLG2, but not TMEM229B, GPNMB, and ITGA8 polymorphism, is associated with Parkinson's disease in a Taiwanese population. Neurobiol Aging. 2018;64(158):e1–e6. PubMed: 29290481. doi:10.1016/j.neurobiolaging.2017.11.016.
13. Ali S, Hoven A, Dress RJ, Schaal H, Alferink J, Scheu. S. Identification of a novel Dlg2 isoform differentially expressed in IFNbeta-producing plasmacytoid dendritic cells. BMC Genomics. 2018;19(1):194. PubMed: 29703139. doi:10.1186/s12864-018-4573-5.
14. Zhu J, Shang Y, Xia Y, Zhang R, Zhang M. An atypical MAGUK GK target recognition mode revealed by the interaction between DLG and KIF13B. Structure. 2016 Nov;24:1876–1885. PubMed: 27642159. doi:10.1016/j.str.2016.08.008.
15. Morrison JA, Pike LA, Sams SB, Sharma V, Zhou Q, Severson JJ, Tan AC, Wood WM, Haugen BR. Thioredoxin interacting protein (TXNIP) is a novel tumor suppressor in thyroid cancer. Mol Cancer. 2014;13:62. PubMed: 24645981. doi:10.1186/1476-4598-13-62.
16. Zubakov D, Stupar Z, Kovacs G. Differential expression of a new isoform of DLG2 in renal oncocytoma. BMC Cancer. 2006;6:106. PubMed: 16640776. doi:10.1186/1471-2407-6-106.

17. Dai C, Xie Y, Zhuang X, Yuan Z. MiR-206 inhibits epithelial ovarian cancer cells growth and invasion via blocking c-Met/AKT/mTOR signaling pathway. Biomed Pharmacother. 2018;104:763–770. PubMed: 29807226. doi:10.1016/j.biopha.2018.05.077.
18. Vecchione A, Belletti B, Lovat F, Volinia S, Chiappetta G, Giglio S, Sonego M, Cirombella R, Onesti EC, Pellegrini P, et al. A microRNA signature defines chemoresistance in ovarian cancer through modulation of angiogenesis. Proc Natl Acad Sci U S A. 2013;110(24):9845–9850. PubMed: 23697367. doi:10.1073/pnas.1305472110.
19. Li Y, Chen H, She P, Chen T, Chen L, Yuan J, Jiang B. microRNA-23a promotes cell growth and metastasis in gastric cancer via targeting SPRY2-mediated ERK signaling. Oncol Lett. 2018;15(6):8433–8441. PubMed: 29805579. doi:10.3892/ol.2018.8374.
20. Quan J, Liu S, Dai K, Jin L, He T, Pan X, Lai. Y. MicroRNA-23a/24-2/27a as a potential diagnostic biomarker for cancer: a systematic review and meta-analysis. Mol Clin Oncol. 2018;8(1):159–169. PubMed: 29387410. doi:10.3892/mco.2017.1492.
21. Su L, Liu M. Correlation analysis on the expression levels of microRNA-23a and microRNA-23b and the incidence and prognosis of ovarian cancer. Oncol Lett. 2018;16(1):262–266. PubMed: 29928410. doi:10.3892/ol.2018.8669.
22. Guo T, Gaykalova DA, Considine M, Wheelan S, Pallavajjala A, Bishop JA, Westra WH, Ideker T, Koch WM, Khan Z, et al. Characterization of functionally active gene fusions in human papillomavirus related oropharyngeal squamous cell carcinoma. Int J Cancer. 2016;139(2):373–382. PubMed: 26949921. doi:10.1002/ijc.30081.
23. Hong S, Li X, Zhao Y, Yang Q, Kong B. 53BP1 suppresses tumor growth and promotes susceptibility to apoptosis of ovarian cancer cells through modulation of the Akt pathway. Oncol Rep. 2012;27(4):1251–1257. PubMed: 22266878. doi:10.3892/or.2012.1641.
24. Hong S, Li X, Zhao Y, Yang Q, Kong B. 53BP1 inhibits the migration and regulates the chemotherapy resistance of ovarian cancer cells. Oncol Lett. 2018;15(6):9917–9922. PubMed: 29928364. doi:10.3892/ol.2018.8596.
25. Singh A, Srivastava AN, Akhtar S, Siddiqui MH, Singh P, Kumar V. Correlation of CD133 and Oct-4expression with clinicopathological and demographic parameters in oral squamous cell carcinoma patients. Natl J Maxillofac Surg. 2018;9(1):8–13. PubMed: 29937653. doi:10.4103/njms.NJMS_60_17.
26. Di J, Boer TD-D, Zusterzeel PL, Figdor CG, Massuger LF, Torensma R. The stem cell markers Oct4A, Nanog and c-Myc are expressed in ascites cells and tumor tissue of ovarian cancer patients. Cell Oncol (Dordr). 2013;36(5):363–374. PubMed: 23928726. doi:10.1007/s13402-013-0142-8.
27. Sun C, Li N, Zhou B, Yang Z, Ding D, Weng D, Meng L, Wang S, Zhou J, Ma D, et al. miR-222 is upregulated in epithelial ovarian cancer and promotes cell proliferation by downregulating P27 (kip1.). Oncol Lett. 2013;6(2):507–512. PubMed: 24137356. doi:10.3892/ol.2013.1393.
28. Xu X, Ayub B, Liu Z, Serna VA, Qiang W, Liu Y, Hernando E, Zabludoff S, Kurita T, Kong B, et al. Anti-miR182 reduces ovarian cancer burden, invasion, and metastasis: an in vivo study in orthotopic xenografts of nude mice. Mol Cancer Ther. 2014;13(7):1729–1739. PubMed: 24825857. doi:10.1158/1535-7163.MCT-13-0982.
29. Chhabra R,R, Dubey NS. Cooperative and individualistic functions of the microRNAs in the miR-23a~27a~24-2 cluster and its implication in human diseases. Mol Cancer. 2010;9:232. PubMed: 20815877. doi:10.1186/1476-4598-9-254.
30. Wang Z, Wei W, Sarkar FH. miR-23a, a critical regulator of "migR"ation and metastasis in colorectal cancer. Cancer Discov. 2012;2(6):489–491. PubMed: 22684455. doi:10.1158/2159-8290.CD-12-0177.
31. Jin AH, Wei ZL. Molecular mechanism of increased sensitivity of cisplatin to ovarian cancer by inhibition of microRNA-23a expression. Int J Clin Exp Med. 2015;8(8):13329–13334. PubMed: 26550261.
32. Gao G, Kasperbauer JL, Tombers NM, Wang V, Mayer K, Smith DI. A selected group of large common fragile site genes have decreased expression in oropharyngeal squamous cell carcinomas. Genes Chromosomes Cancer. 2014;53(5):392–401. PubMed: 24481768. doi:10.1002/gcc.22150.
33. Kim J, So S, Lee HJ, Park JC, Kim JJ, Lee H. DigSee: disease gene search engine with evidence sentences (version cancer). Nucleic Acids Res. 2013;41(Web Server issue):W510–W517. PubMed: 23761452. doi:10.1093/nar/gkt531.
34. Han J, Yu CQ, Shen W. Inhibitory effects of puerarin on invasion and metastasis of oophoroma cells HO-8910. Zhongguo Zhong Xi Yi Jie He Za Zhi. 2009;29(7):632–635. PubMed: 19852298.
35. Gupta S, Iljin K, Sara H, Mpindi JP, Mirtti T, Vainio P, Rantala J, Alanen K, Nees M, Kallioniemi. O. FZD4 as a mediator of ERG oncogene-induced WNT signaling and epithelial-to-mesenchymal transition in human prostate cancer cells. Cancer Res. 2010;70(17):6735–6745. PubMed: 20713528. doi:10.1158/0008-5472.CAN-10-0244.